

A NUMERICAL STUDY OF THE EFFECTS OF LONGWAVE RADIATION AND SURFACE FRICTION ON CYCLONE DEVELOPMENT

MAURICE B. DANARD

University of Waterloo, Waterloo, Ontario, Canada

ABSTRACT

An eight-level primitive equation model has been developed incorporating orography, large-scale release of latent heat, longwave radiation, and surface and internal friction. The clouds and moisture patterns used in the radiation calculations are predicted (i.e., change with time). Drag coefficients vary spatially. Thirty-six-hr predictions are performed over North America for an intense midlatitude winter cyclone.

The inclusion of longwave radiation lowers 300-mb heights by as much as 190 m after 36 hr and significantly improves the forecasts at that level. However, there is little influence at lower levels or on predicted precipitation amounts.

Less intense Highs and Lows result when surface friction is included. In the cyclone area, 1000-mb heights are raised by as much as 110 m after 36 hr. Maximum Ekman layer wind speeds are reduced from about 50 to 25 m/s. However, precipitation amounts are not significantly affected.

1. INTRODUCTION

In a recent paper (Danard 1969b), the author studied the effects of surface friction on cyclone development. The intensity of the sea-level cyclone decreased when friction was introduced but the precipitation amounts were relatively unaffected. It was suggested that the decreased midtropospheric vertical velocities were offset by increased frictionally induced vertical motions in the low levels. However, the model used was quasi-geostrophic and the results, though probably qualitatively correct, may have suffered as a consequence of this restriction.

In another paper (Danard 1969a), the author devised a method of computing longwave radiation from clouds and water vapor in the troposphere. In the cyclone area, longwave radiation was shown to be normally smaller than the release of latent heat. However, the former tends to cool the top of the cloud mass. This has also been noted by Möller (1951), Cox (1969), and others. It was suggested that this destabilizing influence might have important consequences on the dynamics of the cyclone.

The present paper examines the influences of surface friction and longwave radiation on a selected midlatitude cyclone. For this purpose, a multilevel primitive equation numerical prediction model is devised. This is described in section 2. The model includes large-scale release of latent heat, surface and internal friction, and longwave radiation.

Table 1 shows the relative size of the terms in the earth's mean tropospheric heat budget for middle and polar latitudes during January and July. In January, longwave radiation and release of latent heat are the largest contributors. These are included in the model discussed in section 2. In July, absorption of solar radiation is also important. This is probably true in equatorial latitudes during all seasons. Therefore, the numerical model used

in this paper is not so applicable in those instances. Boundary flux (sensible heat transfer from the earth's surface), while apparently a relatively small term overall, may be locally important (e.g., off the east coasts of North America and Asia in winter).

The intense cyclone of Feb. 24–26, 1965, over North America is studied in section 3. Three 36-hr numerical integrations are performed: with longwave radiation and surface friction (RF), excluding radiation but including surface friction (NRF), and including radiation but excluding friction (RNF). Large-scale release of latent heat is incorporated in all three runs.

TABLE 1.—Mean heating during January and July for the region from 30°–70°N and from 1010–200 mb. Units in 10^9 cal/day. (Adapted from Davis 1963)

| Month | Infrared radiation | Solar radiation | Latent heat release | Boundary flux |
|---------|--------------------|-----------------|---------------------|---------------|
| January | –390 | 55 | 190 | 74 |
| July | –490 | 240 | 210 | 86 |

2. THE MODEL

The model has some similarity to that of Smagorinsky et al. (1965) as modified by Manabe et al. (1965) and Miyakoda et al. (1969). The last-named model will hereafter be referred to as the GFDL model. The model described in this paper also uses "sigma" coordinates, proposed by Phillips (1957). Let $\sigma = p/p_s$, where p is the pressure and p_s is the pressure at the earth's surface. The geopotential $\phi = gz$, velocity components u and v , vertical velocity $\dot{\sigma} = d\sigma/dt$, temperature T , and mixing ratio r are computed at the σ -levels shown in figure 1. Clouds and precipitation may occur in any of the four

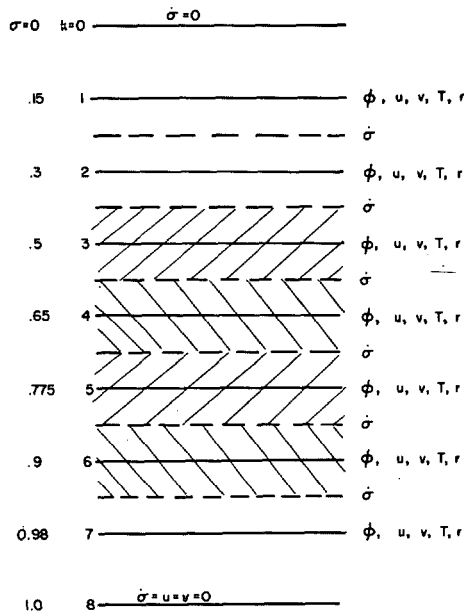


FIGURE 1.—Levels at which various physical quantities are computed. Crosshatching denotes layer in which cloud may exist.

layers centered at $k=3, 4, 5$, and 6 (indicated by crosshatching). Physical processes included are:

1. Orography (adapted from Berkofsky and Bertoni 1955),
2. Large-scale precipitation and release of latent heat,
3. Longwave radiation from water vapor (adapted from Danard 1969a), and
4. Friction at the lower boundary and internal friction.

The system of differential equations to be solved is similar to eq (2A1)–(2A5) of Smagorinsky et al. (1965) and eq (2.2) of Manabe et al. (1965). The equations, in map coordinates for a polar stereographic projection with a cutting plane at 60°N , are

$$\begin{aligned} \frac{\partial}{\partial t} p_s u = & -m^2 \left(\frac{\partial}{\partial x} \frac{p_s u^2}{m} + \frac{\partial}{\partial y} \frac{p_s uv}{m} \right) - p_s \frac{\partial}{\partial \sigma} \dot{\sigma} u \\ & + [f - (vx - uy)/(1.866a^2)] p_s v - m p_s \frac{\partial \phi}{\partial x} \\ & - mRT \frac{\partial p_s}{\partial x} + m^2 K_M \nabla^2 p_s u + F_{vx}, \quad (1) \end{aligned}$$

$$\begin{aligned} \frac{\partial}{\partial t} p_s v = & -m^2 \left(\frac{\partial}{\partial x} \frac{p_s uv}{m} + \frac{\partial}{\partial y} \frac{p_s v^2}{m} \right) - p_s \frac{\partial}{\partial \sigma} \dot{\sigma} v \\ & - [f - (vx - uy)/(1.866a^2)] p_s u - m p_s \frac{\partial \phi}{\partial y} \\ & - mRT \frac{\partial p_s}{\partial y} + m^2 K_M \nabla^2 p_s v + F_{vy}, \quad (2) \end{aligned}$$

$$\begin{aligned} \frac{\partial p_s T}{\partial t} = & -m^2 \left(\frac{\partial}{\partial x} \frac{p_s u T}{m} + \frac{\partial}{\partial y} \frac{p_s v T}{m} \right) - p_s \frac{\partial}{\partial \sigma} \dot{\sigma} T \\ & + \frac{RT\omega}{c_p \sigma} + \frac{p_s}{c_p} (H_L + H_R) + m^2 K_T \nabla^2 p_s T, \quad (3) \end{aligned}$$

$$\begin{aligned} \frac{\partial}{\partial t} p_s r = & -m^2 \left(\frac{\partial}{\partial x} \frac{p_s ur}{m} + \frac{\partial}{\partial y} \frac{p_s vr}{m} \right) - p_s \frac{\partial}{\partial \sigma} \dot{\sigma} r \\ & - p_s C + m^2 K_r \nabla^2 p_s r, \quad (4) \end{aligned}$$

$$\frac{\partial p_s}{\partial t} = -m^2 \left(\frac{\partial}{\partial x} \frac{p_s u}{m} + \frac{\partial}{\partial y} \frac{p_s v}{m} \right) - p_s \frac{\partial \dot{\sigma}}{\partial \sigma}, \quad (5)$$

$$\frac{\partial \phi}{\partial \ln \sigma} = -RT, \quad (6)$$

$$\begin{aligned} p_s \dot{\sigma} = & -(1 - \sigma) \int_0^\sigma m^2 \left(\frac{\partial}{\partial x} \frac{p_s u}{m} + \frac{\partial}{\partial y} \frac{p_s v}{m} \right) d\sigma \\ & + \sigma \int_\sigma^1 m^2 \left(\frac{\partial}{\partial x} \frac{p_s u}{m} + \frac{\partial}{\partial y} \frac{p_s v}{m} \right) d\sigma, \quad (7) \end{aligned}$$

and

$$\omega = \sigma m \left(u \frac{\partial p_s}{\partial x} + v \frac{\partial p_s}{\partial y} \right) - \int_0^\sigma m^2 \left(\frac{\partial}{\partial x} \frac{p_s u}{m} + \frac{\partial}{\partial y} \frac{p_s v}{m} \right) d\sigma. \quad (8)$$

In eq (1)–(4), K_M , K_T , and K_r are eddy diffusivities. The map distortion factor (ratio of the distance on the projection to the distance on the earth) is denoted by m , x and y are orthogonal coordinates on the projection, f is the Coriolis parameter, a is the earth's radius, R is the gas constant, F_{vx} and F_{vy} represent effects of vertical mixing [see eq (10) and (11)], $\omega \equiv dp/dt$, H_L [see eq (9)] and H_R are the rates of input of heat per unit mass due to condensation and longwave radiation, respectively, and C is the rate of decrease of r due to condensation.

The clouds and water vapor used in the radiation calculations change with time as the mixing ratio changes. This should be useful in assessing the role of radiation in cyclone development since the cloud pattern tends to move with the storm. The drag coefficients vary spatially. This permits examining the role of differential friction in atmospheric motions. The above two features were not included in the GFDL model. However, the GFDL model does incorporate physical processes not in the model described here.

The method of computing finite differences is described in appendix I.

Initial data consist of isobaric heights at 1000, 850, 700, 500, and 300 mb, as well as temperatures and dewpoint temperatures at 850, 700, and 500 mb. Data are taken over a 24×28 set of grid points in the horizontal. This is a subset of the array used by the National Meteorological Center, the Canadian Meteorological Service, and the Fleet Numerical Weather Facility. The area covered by the innermost 14×18 set of points is shown in figures 2–10.

The surface pressure is first derived from the 1000-, 850-, and 700-mb heights in the following manner. The D -factor is computed for the three pressure surfaces. This is defined as $(z - z_s)$, where z_s is the height in the standard atmosphere of the same pressure to which the isobaric height z refers. The D -factor at the elevation of the earth's surface is found by quadratic interpolation. This gives the standard atmosphere height corresponding to the surface pressure. The surface pressure is then easily obtained. Next, the temperatures at the σ -surfaces are obtained by inter-

polarization using isobaric heights and temperatures. The temperature is assumed to vary linearly with $\ln p$ between information surfaces. The thickness between two isobaric surfaces gives a mean temperature assumed to apply at the geometric mean of the upper and lower pressures. Thus, the temperature derived from the 500- to 300-mb thickness is applied at 390 mb. At $k=1$ (see fig. 1), the temperature is everywhere initially set equal to the average value at 390 mb. At $k=2$, the initial temperature is half the sum of the actual 390-mb temperature and the average value at 390 mb. Thus, the temperature gradients at $k=2$ are smaller than at 390 mb. This is done because no other temperature data are available at these heights. The hydrostatic equation [eq (6)] is then integrated numerically assuming a linear variation of T and $\ln p$ between σ -surfaces. This gives initial values of ϕ .

For the surfaces $k=3, 4, 5, 6$, and 7 , r is obtained from the initial dewpoint data, assuming $(T-T_d)$ varies linearly with pressure between information surfaces. At $k=1$, r is initially set equal to a constant value of 1.33×10^{-6} . This corresponds to a frostpoint, T_f , of 190°K . Manabe and Möller (1961) noted that T_f is close to this value in the lower stratosphere regardless of latitude or season. The values of r at $k=2$ are obtained initially by interpolation from those at $k=1$ and $k=3$.

The nonlinear balance equation is solved in σ -coordinates to give initial horizontal velocities. This was also done by Shuman and Hovermale (1968). The resulting values of u and v are substituted in eq (7) and (8) to give initial vertical velocities. However, these vertical velocities are not realistic and, as shown in section 3, a number of time steps are needed before satisfactory vertical motions are achieved. This poorly defined initial state is one of the most serious defects in the model.

The calculations are integrated in time for 36 hr using the "leapfrog" method with time steps of 10 min. The boundary values of u , v , ϕ , T , r , and p_s are held fixed. The control of gravity waves propagating inward from the boundary is described below in the discussion on horizontal mixing. Equations (1)–(5) give prognostic values of u , v , T , r , and p_s . The diagnostic equations, eq (7) and (8), yield the new vertical velocities. Equation (6) is then integrated using the predicted temperatures. This results in new values of ϕ .

The grid point values of terrain height obtained from Berkofsky and Bertoni (1955) were slightly smoothed using eq (5) of Shuman (1957) with $\nu=1/2$ where ν is the smoothing element index. The highest grid point heights of the resulting terrain are 6,800 ft over both Colorado and Greenland.

For the radiation calculations, clouds are assumed to exist whenever the relative humidity exceeds the values in the top line of table 2. The author's method of computing longwave radiation (Danard 1969a) is used. The procedure is adapted to sigma coordinates and the existence of a cloud-free space adjacent to the earth's surface (fig. 1). Since the model is essentially a tropospheric one,

TABLE 2.—Critical relative humidities (percent) for existence of cloud (top line) and formation of precipitation (bottom line). (Adapted from Smagorinsky 1960)

| σ -level | 0.5 | 0.65 | 0.775 | 0.9 |
|-----------------|-----|------|-------|-----|
| Cloud | 70 | 74 | 78 | 84 |
| Precipitation | 82 | 84 | 87 | 90 |

only water vapor is considered (i.e., carbon dioxide and ozone are neglected for reasons given in Danard 1969a). The temperature at $k=8$ (the earth's surface) is set equal to the mean sea temperature over the ocean. Over land it is extrapolated from levels 6 and 7. In this model, radiation thus cools the free atmosphere but not the earth's surface directly. Although it would be simple to include, the latter cooling is intentionally omitted to compensate for the absence of solar heating. In the real atmosphere, longwave radiation at night cools the earth's surface which, in turn, cools the adjacent atmosphere by eddy conduction. The surface temperature affects only the radiation calculations. It has no effect on the vertical advection in the thermodynamic equation because of the finite-difference method used (eq A17 of Smagorinsky et al. 1965).

The rate of release of latent heat per unit mass is given by

$$H_L = -L\omega \left(\frac{dr}{dp} \right)_s \Delta_s \quad (9)$$

where L is the latent heat of vaporization, $(dr/dp)_s$ is the rate of change of mixing ratio with pressure in the saturated state, and Δ_s varies linearly from zero to one as the relative humidity varies from the critical values in the bottom line of table 2 to 100 percent. If $\omega > 0$, or if the relative humidity is less than the critical value, $\Delta_s = 0$. The numbers in table 2 are adapted from Smagorinsky (1960) and correspond to his values for 0.8 (top line) and overcast (bottom line) cloud cover. Convective adjustment was not incorporated in the case study described here.

Computational stability necessitates a time step of 10 min in the equations of motion. However, release of latent heat and longwave radiation are diagnostic calculations, and need not be so restricted. Here they are calculated every six time steps and held fixed until the next computation.

The eddy diffusivities in eq (1)–(4) represent real physical processes and also help control computational instability. Grimminger (1941) computed K_r at 700 mb. His values ranged from 3×10^8 to $4 \times 10^{10} \text{ cm}^2/\text{s}$. Murgatroyd (1969) calculated K_M at levels between 700 and 30 mb. His results varied from 2×10^9 to 2×10^{11} . Thus there is a considerable range (up to three orders of magnitude) in computed eddy diffusivities. Phillips (1956) used a value of $10^9 \text{ cm}^2/\text{s}$ for K_M and K_T . Benwell and Bushby (1970) also employed $K_M = 10^9$. Krishnamurti (1969) set

$K_M = 5 \times 10^8$. In this study, the figures used are $K_M = 4 \times 10^9$ and $K_T = K_r = 4 \times 10^8$ cm²/s. The equations of motion [eq (1) and (2)] are nonlinear in the velocity components. Hence, a higher value is used for K_M than for K_T and K_r . In addition, K_M is increased to 4×10^{10} over the outer three grid points. This retards the inward propagation of gravity waves generated at the boundary. A similar procedure was employed by Benwell and Bushby (1970).

In eq (1) and (2), the terms F_{vz} and F_{v_y} are given by

$$F_{vz} = -p_s C_d u_7 V_7 / \Delta z \quad (10)$$

and

$$F_{v_y} = -p_s C_d v_7 V_7 / \Delta z. \quad (11)$$

Here C_d is the spatially variable drag coefficient (Cressman 1960), V_7 is the wind speed at $k=7$ and $\Delta z=1$ km. To avoid oscillations by imposing surface friction impulsively at the start, the drag coefficients are increased linearly from zero to their full values by 6 hr (time step 36) (Danard 1969b). To prevent computational instability, we computed the diffusion terms in eq (1)–(4), as well as eq (10) and (11), from values at the previous, rather than the current, time step.

3. A CASE STUDY

In earlier studies (Danard 1966a, 1966b), the author performed numerical integrations with a quasi-geostrophic model on four cases of intense cyclogenesis. The cyclone for which pressure change predictions were the poorest was chosen for study with primitive-equation model. This was the storm of Feb. 24–26, 1965. This depression has been described as the worst of the century in its area (U.S. Weather Bureau 1965). Up to 25 in. of snow were dumped on southern Ontario. Surface winds reached hurricane force in New York State.

Numerical integrations are performed for 36 hr starting from 1200 GMT, Feb. 24, 1965. All predictions include large-scale release of latent heat. The RF prognoses incorporate longwave radiation and surface friction. The NRF forecasts exclude radiation but include friction. The RNF integrations include radiation but exclude friction. Predicted isobaric heights are obtained by quadratic interpolation from the heights of the σ -surfaces. The former are then smoothed as described in appendix II. However, the other output fields are not smoothed.

The observed 1000-mb charts are shown in figure 2. The cyclone develops rapidly and moves northeastward from Mississippi to Lake Ontario in 36 hr. The High to the northeast also becomes more intense during this period.

Predicted 1000-mb heights at 12, 24, and 36 hr after the initial time are presented in figure 3. All three prognoses (RF, NRF, and RNF) underestimate both the displacement and deepening of the Low. This is likely a consequence of both truncation error and the poorly defined

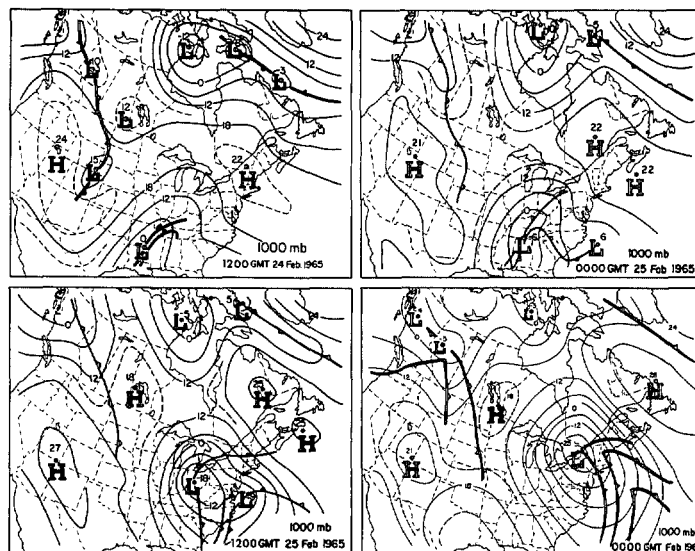


FIGURE 2.—Observed 1000-mb heights. Units: dekameters (dam).

initial state. Moreover, it must be remembered that this cyclone was exceptionally intense. By comparing the RF and NRF predictions, it is seen that longwave radiation has little effect at 1000 mb. On the other hand, exclusion of surface friction (the RNF prognoses) results in more intense Highs and Lows. The effects after 36 hr are evident from figure 4. In the cyclone area, heights are lowered by up to 110 m. These influences of surface friction are similar to those found in an earlier study by the author (Danard 1969b).

Figure 5 shows the 36-hr predicted wind speeds at $\sigma=0.98$ with and without surface friction. This level is approximately 200 m above the ground. The wind speeds over New York State are doubled from 25 m/s to over 50 m/s by excluding surface friction. This is due to intensification of the pressure gradients as well as the absence of retarding frictional forces. One may conclude that had this storm developed over a smooth surface (e.g., the sea) it would have been much more severe.

The initial and final (36 hr later) 500-mb observed charts are given in figure 6. The trough associated with the cyclone forms a cutoff Low of considerable intensity. Meanwhile, the Low originally near Churchill, Manitoba, drifts northward.

Prognoses are shown in figure 7. The predictions succeed in forming a cutoff Low but fail in the displacement of its center. The RF and RNF forecasts are fairly similar. Thus, the effects of surface friction have damped with height. On the other hand, exclusion of longwave radiation (NRF integrations) results in higher 500-mb heights.

The effects of longwave radiation of 300-mb heights may be seen in figure 8. Excluding radiation raises heights everywhere. The large values (up to 190 m) over southeastern Quebec are associated with the relatively warm cloud mass which has blown downwind from the cyclone.

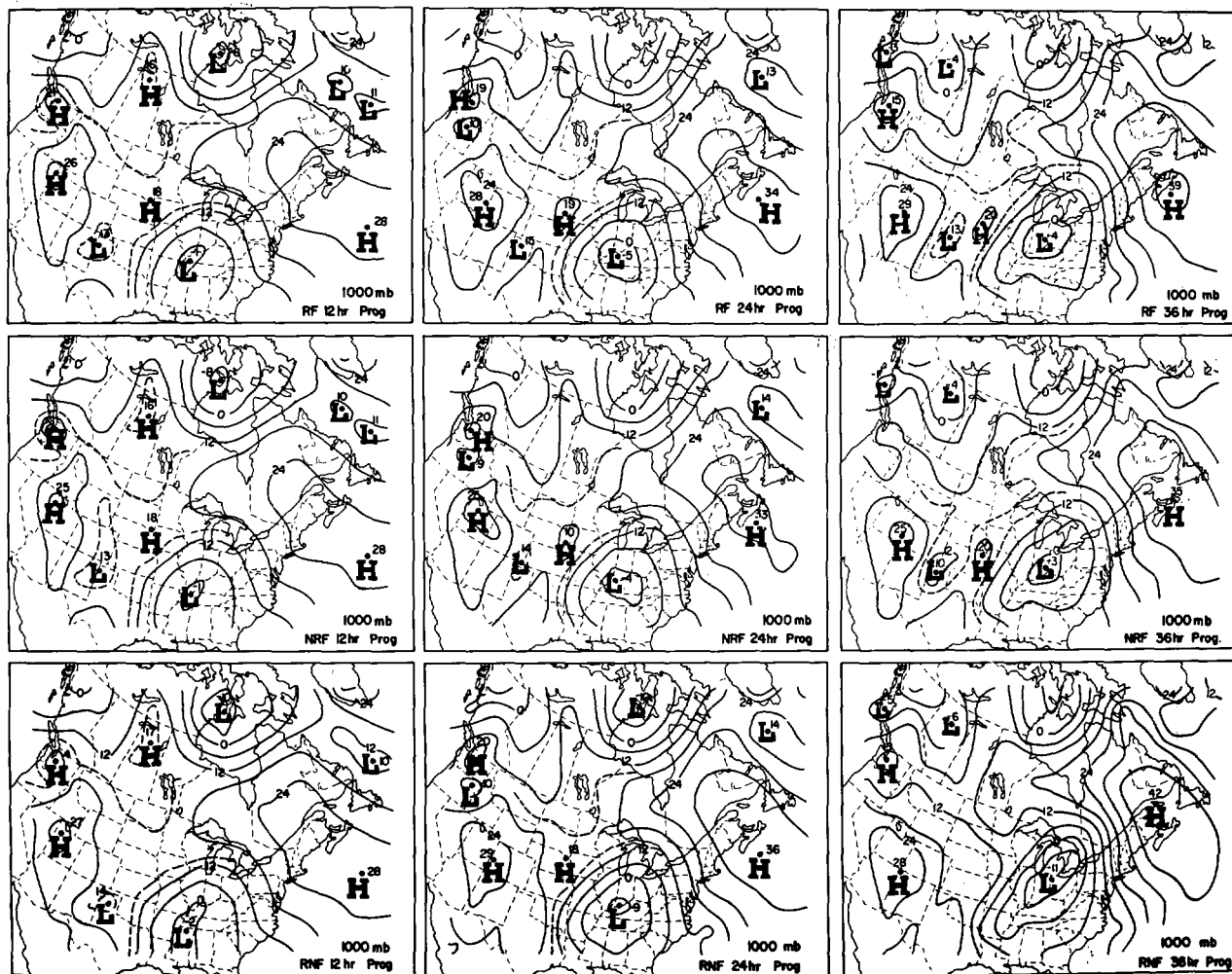


FIGURE 3.—Predicted 1000-mb heights (dam) including longwave radiation and surface friction (RF), excluding radiation but including friction (NRF), and including radiation but omitting friction (RNF). Initial time is 1200 GMT on Feb. 24, 1965.

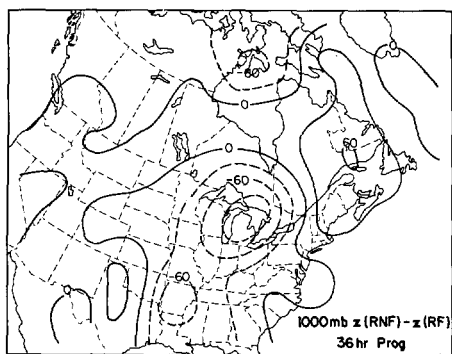


FIGURE 4.—Predicted height differences at 1000 mb (m) without surface friction minus with friction.

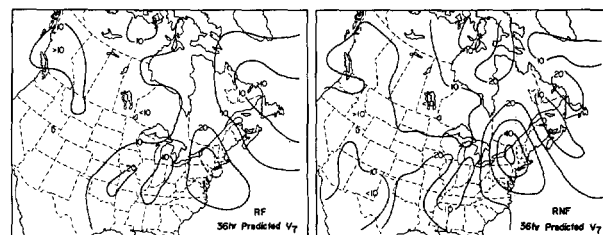


FIGURE 5.—Predicted wind speeds (m/s) at $\sigma = 0.98$ with surface friction and without surface friction.

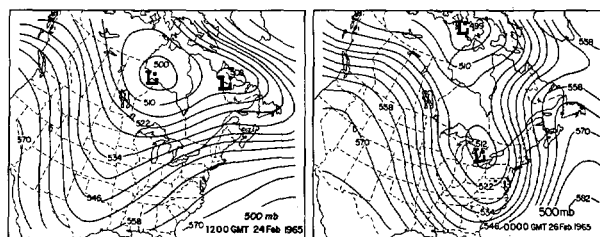


FIGURE 6.—Observed 500-mb heights (dam).

Figure 9 gives the 36-hr predicted wind speeds at $\sigma=0.3$ with and without longwave radiation. Somewhat surprisingly, the speeds are similar in both prognoses. The geostrophic wind corresponding to the height gradient in figure 8 is approximately equal to vector wind

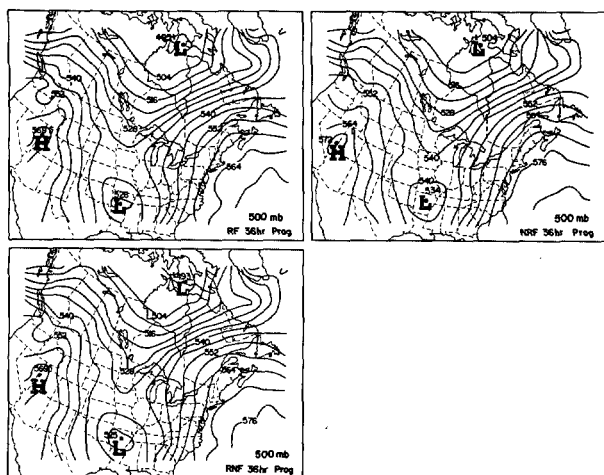


FIGURE 7.—Predicted 500-mb heights (dam)

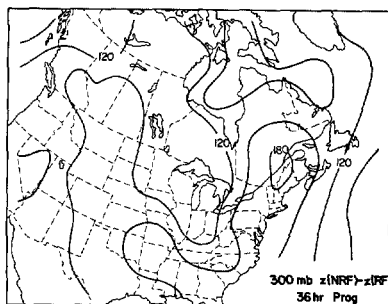
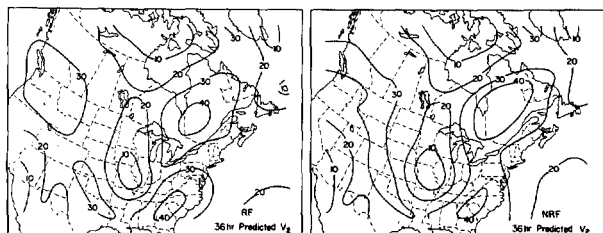


FIGURE 8.—Predicted height differences at 300 mb (m) without radiation minus with radiation.

FIGURE 9.—Predicted wind speeds (m/s) at $\sigma = 0.3$ with radiation and without radiation.

difference when radiation is omitted. Here, this vector difference apparently affects the wind direction appreciably but not its magnitude.

Table 3 shows the mean height changes and errors for the three prognoses. From the 36-hr results, it is seen that all predictions overestimate isobaric heights at lower levels. The RF and RNF forecasts underestimate the 500- and 300-mb heights. Thus, these integrations underestimate the mean troposphere temperatures. On the other hand, the NRF prognosis yields temperatures which are too high. These results are to be expected according to table 1. A model which includes only latent heat release (NRF) has a net heat source. Addition of

TABLE 3.—Mean actual height changes (Δz) and mean height errors (forecast minus observed) for prognoses

| Time | Level | Δz | Prognostic | | |
|-------|-------|------------|------------|-----|-----|
| | | | RF | NRF | RNF |
| 12 hr | (mb) | (m) | (m) | (m) | (m) |
| | 1000 | -9 | 12 | 11 | 12 |
| | 850 | 9 | -3 | -3 | -4 |
| | 700 | 17 | -16 | -9 | -16 |
| | 500 | 22 | -38 | -18 | -38 |
| 24 hr | 300 | 28 | 36 | 75 | 36 |
| | 1000 | -15 | 31 | 29 | 31 |
| | 850 | -2 | 26 | 27 | 26 |
| | 700 | 9 | 13 | 26 | 13 |
| | 500 | 23 | -25 | 16 | -25 |
| 36 hr | 300 | 38 | 19 | 100 | 20 |
| | 1000 | -34 | 51 | 48 | 50 |
| | 850 | -6 | 36 | 37 | 36 |
| | 700 | 12 | 19 | 38 | 19 |
| | 500 | 38 | -35 | 26 | -33 |
| | 300 | 66 | -26 | 100 | -22 |

TABLE 4.—Root-mean-square actual height changes (R_z) and rms height errors (forecast minus observed) for prognoses

| Time | Level | R_z | Prognostic | | |
|-------|-------|-------|------------|-----|-----|
| | | | RF | NRF | RNF |
| 12 hr | (mb) | (m) | (m) | (m) | (m) |
| | 1000 | 47 | 38 | 37 | 41 |
| | 850 | 43 | 39 | 37 | 41 |
| | 700 | 49 | 48 | 44 | 49 |
| | 500 | 64 | 67 | 57 | 67 |
| | 300 | 80 | 83 | 105 | 83 |
| 24 hr | 1000 | 95 | 84 | 82 | 89 |
| | 850 | 88 | 80 | 77 | 85 |
| | 700 | 92 | 90 | 87 | 92 |
| | 500 | 116 | 107 | 103 | 108 |
| | 300 | 148 | 103 | 144 | 105 |
| 36 hr | 1000 | 132 | 115 | 110 | 128 |
| | 850 | 119 | 116 | 111 | 125 |
| | 700 | 134 | 136 | 133 | 141 |
| | 500 | 179 | 162 | 156 | 164 |
| | 300 | 245 | 167 | 197 | 168 |

longwave radiation (RF and RNF) results in a net heat sink.

Table 4 shows the root-mean-square (rms) errors of a persistence forecast (R_z) as well as those of the three numerical integrations. After 36 hr, the NRF prognosis is slightly better than the other two from 1000 to 500 mb, inclusive. On the other hand, addition of longwave radiation (RF and RNF) clearly improves the predictions at 300 mb. Presumably this is because cloud top cooling is important in the upper troposphere. The NRF forecast is better than persistence at all levels. Except at 700 mb, so is the RF prognosis. The RNF integration beats persistence except at 850 and 700 mb. It should be pointed out that interpolation to obtain isobaric heights from those at the σ -surfaces tends to amplify rms errors. The quasi-geostrophic numerical integration performed earlier by the author (1966b) is comparable to the NRF run. Identical initial data were used (section 1). The primitive-equation model (NRF) produced lower rms

TABLE 5.—Mean and rms height differences between prognoses

| Time | Level | Mean (m) | | rms (m) | |
|-------|-------|----------|--------|---------|--------|
| | | NRF-RF | RNF-RF | NRF-RF | RNF-RF |
| 12 hr | (mb) | | | | |
| | 1000 | -1 | 0 | 4 | 7 |
| | 850 | 1 | 0 | 4 | 4 |
| | 700 | 7 | -1 | 10 | 3 |
| | 500 | 20 | 0 | 21 | 3 |
| | 300 | 38 | 0 | 39 | 2 |
| 24 hr | 1000 | -3 | 0 | 9 | 18 |
| | 850 | 1 | 0 | 9 | 12 |
| | 700 | 13 | 0 | 18 | 9 |
| | 500 | 40 | 1 | 43 | 9 |
| | 300 | 81 | 1 | 83 | 6 |
| 36 hr | 1000 | -4 | -2 | 16 | 30 |
| | 850 | 1 | 0 | 16 | 20 |
| | 700 | 19 | 1 | 26 | 16 |
| | 500 | 61 | 2 | 65 | 16 |
| | 300 | 127 | 4 | 129 | 14 |

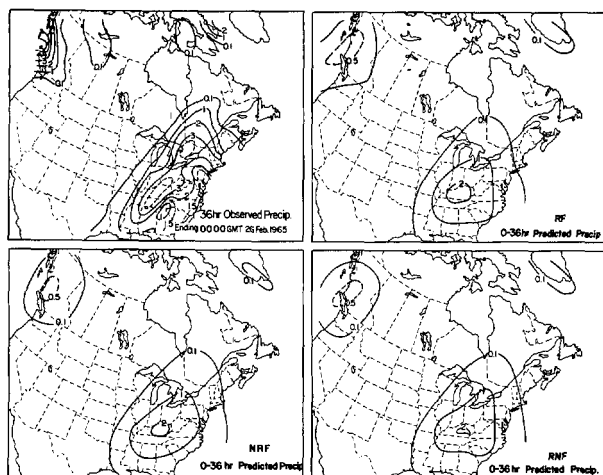


FIGURE 10.—Observed and predicted 36-hr precipitation amounts (cm).

errors at all levels (by 7–23 m) after 36 hr than did the geostrophic model. It is interesting to note that at 500 and 300 mb, the performance of all three prognoses in table 4 improves with time, compared to persistence. This is probably a result of the poorly defined initial state.

Differences between the prognoses are shown in table 5. After 36 hr, the 300-mb heights are raised by an average of 127 m as a result of excluding radiation. On the other hand, there is relatively little effect in the lower troposphere. The effect of surface friction is delineated by the rms height differences. The damping of this influence with height is apparent.

Observed and predicted precipitation patterns are presented in figure 10. The observed amounts represent averages over squares having sides equal to one gridlength (380 km at 60°N). The underestimate of the extremes in all three prognoses is consistent with the underestimate of the cyclone's intensity (see fig. 3). In addition, since

initially $\dot{\sigma} \equiv 0$, it takes a few time steps before vertical velocities and precipitation rates attain appreciable magnitudes.

All three forecast precipitation patterns are quite similar. The resemblance between the RF and RNF predictions has been noted before (see section 1 for explanation). However, the similarity between the RF and NRF prognoses was not anticipated. A possible explanation is the following. Most of the cloud mass is in the warm air so that cloud top cooling tends to reduce horizontal temperature contrasts (see Danard 1969a) and large-scale upward motion. This is offset by the tendency for destabilization to augment the vertical velocity. Inclusion of convective adjustment would probably not have significantly altered the results. The author has calculated the precipitation resulting from radiational cooling of a cloud mass originally having a pseudoadiabatic lapse rate (Danard 1969a). Amounts were only of the order of 1 mm in 12 hr. However, the problem of convective adjustment deserves further study.

4. CONCLUDING REMARKS

The main purpose of this paper has been to investigate the influences of longwave radiation and surface friction during the development of an intense midlatitude cyclone. After 36 hr., radiation lowers 300-mb heights by as much as 190 m but has relatively little influence on wind speeds in the upper troposphere. Friction raises 1000-mb heights near the cyclone by as much as 110 m and decreases wind speeds in the Ekman layer by as much as 25 m/s. However, neither process has much effect on precipitation amounts.

In addition to understanding the role of the above physical processes, one is interested in producing accurate forecasts. Here, there is room for improvement. However, the forecast inaccuracies were in part due to the unusual character of the cyclone selected for study. The cyclone was very intense and was deliberately chosen because it was poorly handled by a geostrophic model. A version of the primitive-equation model with the grid size halved to reduce truncation error is being developed for a smaller area. In addition, work is proceeding on an improved initialization scheme based on Nitta and Hovermale's (1969) procedures.

APPENDIX I: FINITE DIFFERENCES

The horizontal finite differences employed are similar to those of Gates (1968). Using the nomenclature of figure 11, if ψ is any function,

$$\frac{\partial \psi}{\partial x} = \left(\frac{\psi_1 + \psi_2 + \psi_3}{3} - \frac{\psi_7 + \psi_8 + \psi_9}{3} \right) / 2h \quad (12)$$

where h is the grid distance on the projection (381 km). Thus the function is averaged in the y -direction before its difference is taken in the x -direction. A similar equation

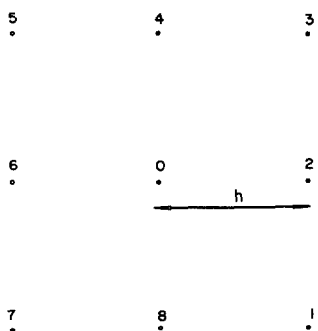


FIGURE 11.—Grid points referred to in eq (12) and (13).

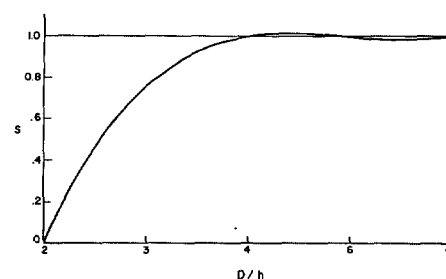


FIGURE 12.—Ratio of amplitude of smoothed to unsmoothed fields after applying eq (15).

holds for $\partial\psi/\partial y$. The vertical finite differences are virtually identical to those of Smagorinsky et al (1965). The finite difference equation for the Laplacian [see eq (1)–(5)] is

$$\nabla^2\psi = (\psi_2 + \psi_4 + \psi_6 + \psi_8 - 4\psi_0)/2h^2 + (\psi_3 + \psi_5 + \psi_7 + \psi_1 - 4\psi_0)/4h^2. \quad (13)$$

Equation (13) is based on the smoothing operators of Shuman (1957). Two-gridlength waves are smoothed more than any other longer wavelength.

APPENDIX II: SMOOTHING THE OUTPUT (ISOBARIC HEIGHTS)

Consider the one-dimensional field

$$\psi = A_0 + A_1 \cos \frac{2\pi x}{D} \quad (14)$$

where A_0 , A_1 , and D are constants (D is the wavelength). Suppose ψ is known at discrete grid points x_i separated by a grid distance h . Consider the result of applying a symmetric 7-point operator to ψ to obtain the smoothed field, $\bar{\psi}$:

$$\bar{\psi}_i = a_0\psi_i + a_1(\psi_{i-1} + \psi_{i+1}) + a_2(\psi_{i-2} + \psi_{i+2}) + a_3(\psi_{i-3} + \psi_{i+3}). \quad (15)$$

The constants a_0 , a_1 , a_2 , and a_3 determine the response characteristics of the smoothing operator. Let S denote the ratio of the amplitude of the smoothed field, $\bar{\psi}$, to that of the ψ field (A_1). The requirements that $S=0$ for $D/h=2$ and $S=1$ for $D/h=4, 6$, and ∞ yield $a_0=3/4$, $a_1=5/24$, $a_2=-1/8$, and $a_3=1/24$.

The curve of S versus D/h is given in figure 12. Two-gridlength waves are completely removed. The smoothing operator has $S>1$ for $4<D/h<6$. However, the maximum amplification is only 1.6 percent at $D/h=4.62$.

Furthermore, $S<1$ for $6<D/h<\infty$, but the maximum damping is again only 1.6 percent at $D/h=9.48$. The near unity values of S for short waves (say $4 \leq D/h < 12$) is considered desirable in this study of cyclogenesis.

The smoothing operator is applied to two-dimensional fields by first smoothing in the x -direction. This result is then smoothed in the y -direction.

ACKNOWLEDGMENTS

This research was supported by the Canadian Meteorological Service and the National Research Council of Canada. The author expresses his gratitude to Stanley Alleyne and Hans Wobbe, without whose computer programming assistance this project would probably not have been feasible. Barry MacDonald and Stephen Clodman were involved in programming the calculation of radiation and initial surface pressure, respectively. Special thanks are due the Computing Center of the University of Waterloo for their cooperation in executing the program. This paper was typed by Mrs. Charlotte Weber. The figures were drawn by Mrs. Jackie Chen.

REFERENCES

- Benwell, G. R. R., and Bushby, F. H., "A Case Study of Frontal Behaviour Using a 10-level Primitive Equation Model," *Quarterly Journal of the Royal Meteorological Society*, Vol. 96, No. 408, London, England, Apr. 1970, pp. 287–296.
- Berkofsky, Louis, and Bertoni, Eugene A., "Mean Topographic Charts for the Entire Earth," *Bulletin of the American Meteorological Society*, Vol. 36, No. 7, Sept. 1955 pp. 350–354.
- Cox, Stephen K., "Radiation Models of Midlatitude Synoptic Features," *Monthly Weather Review*, Vol. 97, No. 9, Sept. 1969, pp. 637–651.
- Cressman, George P., "Improved Terrain Effects in Barotropic Forecasts," *Monthly Weather Review*, Vol. 88, Nos. 9–12, Sept.–Dec. 1960, pp. 327–342.
- Danard, Maurice B., "A Quasi-Geostrophic Numerical Model Incorporating Effects of Release of Latent Heat," *Journal of Applied Meteorology*, Vol. 5, No. 1, Feb. 1966a, pp. 85–93.
- Danard, Maurice B., "Further Studies With a Quasi-Geostrophic Numerical Model Incorporating Effects of Released Latent Heat," *Journal of Applied Meteorology*, Vol. 5, No. 4, Aug. 1966b, pp. 388–395.
- Danard, Maurice B., "A Simple Method of Including Longwave Radiation in a Tropospheric Numerical Prediction Model," *Monthly Weather Review*, Vol. 97, No. 1, Jan. 1969a, pp. 77–85.
- Danard, Maurice B., "Numerical Studies of Effects of Surface Friction on Large-Scale Atmospheric Motions," *Monthly Weather Review*, Vol. 97, No. 12, Dec. 1969b, pp. 835–844.

- Davis, Paul A., "An Analysis of the Atmospheric Heat Budget," *Journal of the Atmospheric Sciences*, Vol. 20, No. 1, Jan. 1963, pp. 5-22.
- Gates, W. Lawrence, "A Numerical Study of Transient Rossby Waves in a Wind-Driven Homogeneous Ocean," *Journal of the Atmospheric Sciences*, Vol. 25, No. 1, Jan. 1968, pp. 3-22.
- Grimminger, G., "The Intensity of Lateral Mixing in the Atmosphere as Determined From Isentropic Charts," *Bulletin of the American Meteorological Society*, Vol. 22, No. 5, May 1941, pp. 227-233.
- Krishnamurti, Tiruvalem N., "An Experiment in Numerical Prediction in Equatorial Latitudes," *Quarterly Journal of the Royal Meteorological Society*, Vol. 95, No. 405, London, England, July 1969, pp. 594-620.
- Manabe, Syukuro, and Möller, Fritz, "On the Radiative Equilibrium and Heat Balance of the Atmosphere," *Monthly Weather Review*, Vol. 89, No. 12, Dec. 1961, pp. 503-532.
- Manabe, Syukuro, Smagorinsky, Joseph, and Strickler, Robert F., "Simulated Climatology of a General Circulation Model With a Hydrologic Cycle," *Monthly Weather Review*, Vol. 93, No. 12, Dec. 1965, pp. 769-798.
- Miyakoda, Kikuro, Smagorinsky, Joseph, Strickler, Robert F., and Hembree, G. D., "Experimental Extended Predictions With a Nine-Level Hemispheric Model," *Monthly Weather Review*, Vol. 97, No. 1, Jan. 1969, pp. 1-76.
- Möller, Fritz, "Long-Wave Radiation," *Compendium of Meteorology*, American Meteorological Society, Boston, Mass., 1951, pp. 34-49.
- Murgatroyd, R. J., "Estimations From Geostrophic Trajectories of Horizontal Diffusivity in the Mid-Latitude Troposphere and Lower Stratosphere," *Quarterly Journal of the Royal Meteorological Society*, Vol. 95, No. 403, London England, Jan. 1969, pp. 40-62.
- Nitta, Takashi, and Hovermale, John B., "A Technique of Objective Analysis and Initialization for the Primitive Forecast Equations," *Monthly Weather Review*, Vol. 97, No. 9, Sept. 1969, pp. 652-658.
- Phillips, Norman A., "The General Circulation of the Atmosphere: A Numerical Experiment," *Quarterly Journal of the Royal Meteorological Society*, Vol. 82, No. 352, London, England, Apr. 1956, pp. 123-164.
- Phillips, Norman A., "A Coordinate System Having Some Special Advantages for Numerical Forecasting," *Journal of Meteorology*, Vol. 14, No. 2, Apr. 1957, pp. 184-185.
- Shuman, Frederick G., "Numerical Methods in Weather Prediction: II. Smoothing and Filtering," *Monthly Weather Review*, Vol. 85, No. 11, Nov. 1957, pp. 357-361.
- Shuman, Frederick G., and Hovermale, John B., "An Operational Six-Layer Primitive Equation Model," *Journal of Applied Meteorology*, Vol. 7, No. 4, Aug. 1968, pp. 525-547.
- Smagorinsky, Joseph, "On the Dynamical Prediction of Large-Scale Condensation by Numerical Methods," *Geophysical Monograph* No. 5, American Geophysical Union, Washington, D.C., 1960, pp. 71-78.
- Smagorinsky, Joseph, Manabe, Syukuro, and Holloway, J. Leith, Jr., "Numerical Results From a Nine-Level General Circulation Model of the Atmosphere," *Monthly Weather Review*, Vol. 93, No. 12, Dec. 1965, pp. 727-768.
- U.S. Weather Bureau, Office of Climatology, "Weatherwatch," *Weatherwise*, Vol. 18, No. 2, Apr. 1965, pp. 88-102.

[Received December 2, 1970; revised March 1, 1971]